Colloids and Surfaces B: Biointerfaces 175 (2019) 56–64

Contents lists available at ScienceDirect

Colloids and Surfaces B: Biointerfaces

journal homepage: www.elsevier.com/locate/colsurfb

Rational design of polymer-lipid nanoparticles for docetaxel delivery

Juan M.R Albano[a,b], Lígia Nunes de Morais Ribeiro[c], Verônica Muniz Couto[c], Mariana Barbosa Messias[c], Gustavo Henrique Rodrigues da Silva[c], Márcia Cristina Breitkreitz[d], Eneida de Paula[c], Monica Pickholz[a,b,*]

[a] Departamento de Física, Facultad de Ciencias Exactas y Naturales, Universidad de Buenos Aires, Buenos Aires, Argentina
[b] Instituto de Física de Buenos Aires (IFIBA), CONICET-Universidad de Buenos Aires, Buenos Aires, Argentina
[c] Biochemistry and Tissue Biology Department, Institute of Biology, University of Campinas – UNICAMP, Campinas, São Paulo, Brazil
[d] Institute of Chemistry, University of Campinas - UNICAMP, PO Box 6154, 13083-970 Campinas, SP, Brazil

ARTICLE INFO

Keywords:
Rational design
Nanocarrier
Docetaxel
Drug delivery system
Cetyl palmitate
Poloxamer

ABSTRACT

In this work, a stable nanocarrier for the anti-cancer drug docetaxel was rational designed. The nanocarrier was developed based on the solid lipid nanoparticle preparation process aiming to minimize the total amount of excipients used in the final formulations. A particular interest was put on the effects of the polymers in the final composition. In this direction, two poloxoamers -Pluronic F127 and F68- were selected. Some poloxamers are well known to be inhibitors of the P-glycoprotein efflux pump. Additionally, their poly-ethylene-oxide blocks can help them to escape the immune system, making the poloxamers appealing to be present in a nanoparticle designed for the treatment of cancer. Within this context, a factorial experiment design was used to achieve the most suitable formulations, and also to identify the effects of each component on the final (optimized) systems. Two final formulations were chosen with sizes < 250 nm and PDI < 0.2. Then, using dynamic light scattering and nanotracking techniques, the stability of the formulations was assessed during six months. Structural studies were carried on trough different techniques: DSC, x-ray diffraction, FTIR-AR and Molecular Dynamics. The encapsulation efficiency of the anticancer drug docetaxel (> 90%) and its release dynamics from formulations were measured, showing that the polymer-lipid nanoparticle is suitable as a drug delivery system for the treatment of cancer.

1. Introduction

Cancer, and the many issues associated with it, still have a significant impact on public health, in spite of the advances in diagnosis and treatment of the last decades [1]. Several classes of drugs have been used to treat different kinds of neoplastic diseases. In particular, the antineoplastic taxane Docetaxel (DTX) is indicated for the treatment of lung, breast, prostate and colorectal cancer [2–4]. The pharmacological mechanism of DTX, as well as its precursor, paclitaxel (PTX) [4], is the inhibition of microtubules depolymerization in the G2 / M cell-cycle phases [5,6]. Compared with PTX, docetaxel is more efficient and shows improved efficiency when used in association to other chemotherapeutic agents such as doxorubicin [7].

Most of these drugs are administered intravenously [8] and in the case of DTX the available commercial formulations contain high amounts of excipients in order to increase drug solubility [9]. Furthermore, many side effects are associated DTX administration, leading to the need of rigorous dosage control [8,10,11]. Aiming to improve DTX pharmacokinetics and bioavailability, different pharmaceutical forms solutions have arisen [12–14]. In particular, encapsulation in nanoparticles has shown to improve the therapeutic efficiency and increase the safety of chemotherapeutic agents [15,16]. In this direction, the use of polymer-lipid drug delivery systems (DDS) - such as solid lipid nanoparticles (SLN)- to treat cancer would have a lot of advantages, such as the control of adverse reactions, higher efficiency, improved pharmacokinetics and body distribution [17–19].

A SLN-like formulation containing DTX could, for instance, increase its *in vivo* tolerability and also increase drug accumulation inside the tumor [17], where angiogenic factors are not adequately regulated, producing a defective vascular architecture, with fenestrations and capillary leaks [20]. In fact, the interstitial liquid depuration inside the tumor is also inadequate, since the lymphatic system is badly distributed in the tissue [20]. As a result, sub-micrometric particles, tend to accumulate in the tumor and be retained there [21], an effect known as “Enhanced Permeability and Retention effect” (EPR) [22]. A well-designed nanoparticle system could take advantage on the EPR effect to

* Corresponding author at: Departamento de Física, Facultad de Ciencias Exactas y Naturales, Universidad de Buenos Aires, Buenos Aires, Argentina.
E-mail address: monicapickholz@gmail.com (M. Pickholz).

https://doi.org/10.1016/j.colsurfb.2018.11.077
Received 10 July 2018; Received in revised form 2 November 2018; Accepted 28 November 2018
Available online 28 November 2018
0927-7765/

achieve high concentrations inside the neoplastic tissue [23].

SLN can be formulated using a wide variety of lipids, such as cetyl palmitate (CP), fatty acids, mono-, di- and triglycerides, glycerides mix, or waxes, being stabilized with biocompatible surfactants (ionic or non-ionic) agents, such as poloxamers (PL) [24]. Poloxamers, commercially known as Pluronic, are non-ionic linear tri-block copolymers of polyethylene oxide (PEO) and polypropylene oxide (PPO) [25]. Poloxamers can play an active role in a formulation, besides their tensoactive properties [26]. Experimental studies demonstrated that PLs could sensitize multi drug resistant (MDR) neoplastic cells increasing the cytotoxic activity of drugs [27,28]. Multidrug resistance is considered the crucial cause of failure in the treatment of patients with cancer and infectious diseases [29]. The phenotype of neoplastic MDR-cells is associated to the overexpression of membrane proteins from the ATP-dependent transporter proteins super family, or "ATP-Binding Cassette transporters" [30]. This proteins, such as P-glycoprotein (P-gp), produce the extrusion of drugs from the cells [31–33]. Poloxamers inhibit such efflux proteins so that a formulation with high PLs could provide lower drug resistance [34]. Briefly, the inhibition mechanism of the poloxamers over P-gp involves, at least in part, changes in the lipid microenvironment that leads to suppression of ATPase activity and interaction with the drug [35]. Furthermore, due to the polyethylene oxide blocks on the PLs molecular structure, nanoparticles developed with this polymer could present *stealth* properties, thus escaping the immune system and reaching longer circulation times on the bloodstream [36–40].

In this work, we aimed to rational design a novel SLN-like nanoparticle for the delivery of DTX. In particular, we increased the relative concentration of PLs while decreasing the amount of lipids in the formulation, using a factorial design. As a result, two optimized polymer-lipid formulations were obtained, with enhanced encapsulation efficiency and sustained release for docetaxel, which were then physiochemically characterized and tested for shelf-stability.

2. Materials and methods

2.1. Sample preparation

Docetaxel was donated by Cristália Prod. Quim. Farm. Ltda (Itapira, Brazil), Pluronic F68, F127 and cetyl palmitate (CP) were supplied by Sigma-Aldrich Chem. Co. (St Louis, USA). Deionized water (18 MΩ) was obtained from an Elga USF Maxima Ultra-Pure water purifier.

Formulations were composed of CP, F127 and F68. Concisely, a blend of these components was diluted in ethanol, at 65 °C (above the melting point of CP), under magnetic stirring. The mixture was stirred until solvent evaporation, and complete homogenization was achieved. When appropriated, DTX was incorporated to the blend. Simultaneously, deionized water was heated to the same temperature of the blend and dropped over it under high-speed agitation (10,000 rpm) for two minutes with an Ultra-Turrax blender (IKA WerkeStaufen, Germany). The resulting microemulsion was subsequently sonicated for 30 min in a Vibracell tip sonicator (Sonics and Mat. Inc., Danbury, USA) operated at 500 W and 20 kHz, with 30 s (on/off) cycles alternation. The resultant nano-emulsion was immediately cooled to room temperature, to form the nanoparticles.

2.2. Factorial design

In order to investigate the influence of the F127 and F68 surfactants and the drug load on the critical quality attributes (CQA) size, polydispersity (PDI) and zeta potential, a 2^3 factorial design with triplicate in the central point, was carried out. The range of variation of each excipient was determined by previous experiments performed by our group and will be discussed below in the preliminary studies section. The analysis of variance (ANOVA, 95% confidence level) indicated the significant variables to be used in the polynomial fit and the lack of fit was tested. Design Expert 11 software (Minneapolis, USA) was used for data treatment. The models were then used to search for the combination of the experimental factors that provided size lower than 250 nm, PDI lower than 0.2 and maximized the absolute value of Z-potential. Table S1of the supplementary material shows the factor and levels used in the final factorial design.

2.3. Determination of particle´s size, polydispersity, zeta potential and concentration

A dynamic light scattering (DLS) equipment (Nano ZS90 analyzer - Malvern Instruments, UK) was used to determine the hydrodynamic diameter (size), polydispersity index (PDI) and zeta potential (ZP) of the nanoparticles. For determination of the number of particles in the formulation, a NS300 Nanotracking analysis instrument (NanoSight, Amesbury, UK), equipped with a 532 nm laser was used. In both cases, samples were diluted in deionized water (n = 3) for measurements.

2.4. Encapsulation efficiency (%EE)

The quantification of DTX was performed by high performance liquid chromatography (HPLC) using a PS-210 ProStar HPLC (Varian Inc., Palo Alto, USA) equipped with a PS 325 UV–VIS detector, a PS 210 solvent delivery module and Galaxy Workstation software for data collection). The column was a Gemini® 5 µm, C18, 110 Å, with 150 x 4.6 mm (Phenomenex®, Torrance, USA) with flux of 1 mL.min^{-1}. The mobile phase was composed of a mixture of water and acetonitrile (50:50 v/v). The injection volume was 30 µL and the absorbance was followed in 230 nm. The total amount (100%) of DTX present in the nanoparticle suspension (DTX_{total}) was determined by diluting the samples in the mobile phase (n = 3) [41]. The DTX%EE was determined by the ultrafiltration-centrifugation method, using cellulose filters (30 kDa, Millipore). The amount of free DTX (DTX_{free})in the filtrate was quantified by HPLC, and the percentage of encapsulated DTX and drug loading were calculated according to Eqs. (1) and (2) respectively [42–44].

$$\%EE = \frac{DTX\ total\ -\ DTX\ free}{DTX\ total} \cdot 100 \quad (1)$$

$$\%Drug\ loading = \frac{Weight\ of\ encapsulated\ DTX}{Weight\ of\ nanoparticles} \cdot 100 \quad (2)$$

2.5. Transmission Electron Microscopy (TEM)

Morphological analysis was carried out for the samples, by TEM. Uranyl acetate (2%) was added to the diluted samples providing contrast. Then, the aliquots were deposited onto copper grids coated with a carbon film and dried at room temperature. After drying, micrographs of the samples were appreciated using a JEOL 1200 EXII microscope operated at 80 kV.

2.6. Release kinetics experiments

The in vitro release of DTX incorporated in the polymer-lipid nanoparticles was studied using a Franz Diffusion Cell, with a donor solution composed of 5 mM phosphate-buffered saline (PBS, pH 7.4) with Tween 80 at 5% to ensure the sink condition - at 37 °C to simulate physiological condition - separated by a standard regenerated cellulose membrane (Spectrapore® dialysis membrane, 12–14 Kilodalton pore size) (n = 2). A solution of DTX in H_2O: ethanol (50:50) plus 5% Tween 80 was used as control. Serial sampling was performed at specified time intervals (0.15, 0.30, 0.45, 1, 2, 4, 6, 8, 22, 24 h) by removing 200 µL of the receptor compartment and replacing it with the fresh medium, to maintain the sink condition. The amount of DTX in the acceptor compartment was quantified by HPLC.

2.7. Differential scanning calorimetry (DSC)

DSC thermograms were collected in a DSC 2910 Differential Scanning Calorimeter (TA Instruments, USA), coupled with the Thermal Solutions v.1.25 software (TA Instruments, USA). The samples were freeze-dried before analysis. The experimental condition was a ramp of 10 °C.min^{-1}, ranging from 20 to 150 °C. Samples of the optimized nanoparticle formulations prepared without and with docetaxel, and their main components (CP, PLs and DTX) were run.

2.8. X-Ray diffraction analysis (XDR)

Powder X-ray diffraction (XRD) data were obtained in a Shimadzu XRD7000 diffractometer (Tokyo, Japan), using a Cu-Kα source, with a scan step of 2° min − 1, between 2θ values and range from 5 °C to 50 °C. Freeze-dried samples of the optimized formulations, prepared with and without DTX, and their main components (CP, PLs and DTX) were run.

2.9. Physicochemical stability study

The physicochemical stability of the formulations was monitored during 6 months, at fridge temperature (5 ± 2 °C). The analyzed parameters were: nanoparticle size (nm), PDI and ZP (mV). Analysis of variance (ANOVA, 95% confidence level) was used to compare intergroups significant differences, regarding the initial time measurements.

2.10. Molecular dynamics simulations

MD simulations were carried out at Coarse Grain (CG) level. The CG models were based on Martini Force Field (MFF) [45]. The Martini CG model allows a systematic representation of molecules in terms of few building blocks (CG beads) that can be used in a broad range of biomolecular applications [46]. Within MFF many kinds of water models and lipids molecules are fully parameterized [45]. In this direction, based on parameters used in lipids, we built a CG model for cetyl palmitate, in order to test the interaction of the drug with a hydrophobic core similar to that of the prepared polymer-lipid nanoparticle (See Supplementary Material). For the drug model, we choose to use a previous validated model of paclitaxel reported in literature given it´s similar structure to DTX [47]. Three simulations of 2 μs were performed, taking into account different initial conditions. All CG MD simulations were performed using GROMACS 5.0 software [46]. A cut-off of 12 Å was applied for the Lennard-Jones (LJ) and electrostatic interactions. We have carried out the simulations within an ensemble of constant number of molecules, pressure and temperature (NPT) within periodic boundary conditions. The pressure and temperature were kept constant (P = 1 bar and T = 298 K) using the Berendsen thermostat and barostat [48] with a coupling constant of 0.3 ps for temperature and pressure, and compressibility of 3.10^{5} bar $^{-1}$. A time step of 10 fs was used [48,49].

3. Results and discussion

3.1. Preliminary studies

In this work, novel polymer-lipid nanoparticles were developed, based on the preparation method used for SLN [50]. We firstly explored the possibility of formulating a nanoparticle using low amounts of excipients, that would reduce the toxicity associated with DTX formulations administration [8,10,11]. In this direction, we framed our experiments in an initial factorial design that could help us understand the influence of each component and develop a rational formulation. In these preliminary studies, CP levels from 1 to 3% w/v and total polymers from 1 to 5% w/v were tested. Notice that CP concentration was significantly lower than the 4–10% w/v commonly used in the preparation of SNL [51–53]. Additionally, the upper limit of 5% w/v of total polymer was set considering its reported toxicity above this concentration [54]. In these pilot experiments we also tested the feasibility of incorporating all the components directly into the lipid phase of the formulation, due to their similar melting point. The lipid phase is commonly heated up to 10 °C above the melting point of the major lipid component (CP = 55 °C) at the beginning of nanoparticle preparations. This modification of the process was explored in order to incorporate the polymer to the lipid matrix so it would be an initial polymer-lipid matrix.

Table S2 of the supplementary material, shows the results of this first set of formulations designated with the letter T, (T1 to T11). In formulations T1, T3, and T5 to T11, none of the parameters (size, PDI and z-potential) were within the expected range and the systems proved to be unstable, presenting phase separation in the first days after preparation. The results with T2 and T4 (both containing 1% w/v CP) were better: these formulations were visually stable in the first weeks after preparation, with sizes around 250 nm, low polydispersion (PDI ~ 0.250) and negative ZP values.

3.2. Factorial design

Factorial design applied to formulation development allows to minimize the number of required experiments to capture relevant information, including interactions among factors. With the information obtain in the preliminary studies, we elaborated a 2^3 factorial design with three central points, using a fixed 1% w/v of CP concentration, and explored the effects of the two polymers: F127 and F68, and the DTX loading. Taking into account the results of the initial experiments, we set polymers w/v in the range of 0.5–1.5%. For DTX, we chose to explore a concentration ranging from 0.02% to 0.16% w/v, since its most commonly used clinical doses is 0.08% w/v [55]. The results of this factorial design are summarized in Table 1.

All formulations were found to be stable, except for P3 and P10 that showed phase separation approximately a week after the first DLS measurements. As shown in Fig. S1 of the supplementary material, while P10 clearly precipitate at the bottom of the recipient, P3 presented to the naked eye, a denser fraction at the top of the phase separation. These formulations carried the maximum amount of polymers and the extreme lower (P3 = 0.02%) and higher (P10 = 0.16%) DTX concentrations. This result will be confirmed by the factorial design results shown in the next section.

Linear models were built relating the experimental factors to each of the responses (size, PDI and ZP). It was observed that models slightly deviated from linearity, therefore a curvature term was added (calculated as the difference between the average points of the factorial and the experimental central points). This allowed to achieve suitable predictive capability of the models without additional experiments. Tables S3 to S5 (Supplementary material) show the significant coefficients of

Table 1
2^3 Factorial design for SLN formulations containing docetaxel (DTX), Pluronics F127 (F127) and 68 (F68), with triplicate at the central points. Values of the responses: size, PDI and z-potential are given. P3 and P10 were not stable.

Formulation	DTX (%)	F127 (%)	F68 (%)	Size (nm)	PDI	Z-potential (mV)
P1	0.02	1.5	0.5	220.6	0.145	−2.28
P2	0.02	0.5	1.5	230.7	0.136	−6.12
P3	0.02	1.5	1.5	279.8	0.196	−5.58
P4	0.02	0.5	0.5	212.3	0.172	−4.37
P5	0.09	1	1	217.7	0.149	−3.89
P6	0.09	1	1	212.0	0.173	−6.80
P7	0.09	1	1	213.5	0.158	−6.17
P8	0.16	1.5	0.5	228.5	0.250	−4.56
P9	0.16	0.5	0.5	243.4	0.239	−6.84
P10	0.16	1.5	1.5	285.0	0.297	−5.74
P11	0.16	0.5	1.5	238.0	0.189	−6.45

paration of SNL [51–53]. Additionally, the upper limit of 5% w/v of

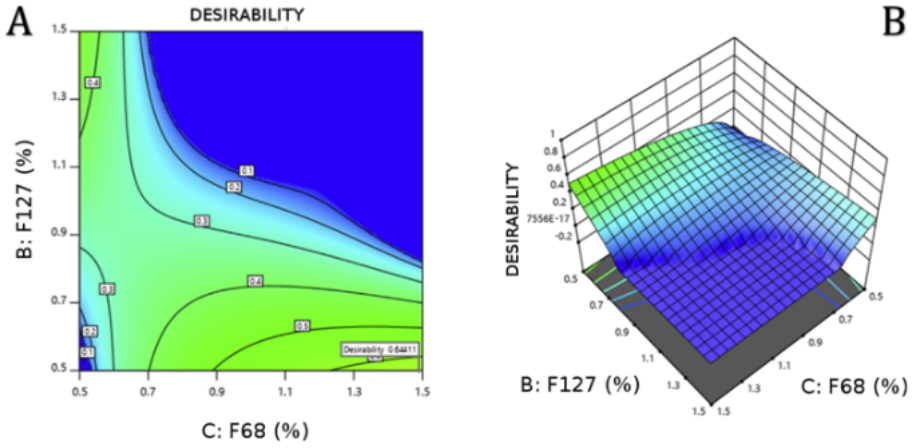

Fig. 1. 2D (A) and 3D (B) desirability plots considering the responses: size, PDI and ZP.

each model, the confidence interval and the curvature term (Ctr Pt). These models were used to predict the experimental conditions to reach: particles size below 250 nm, PDI lower than 0.2 and to maximize the absolute values of zeta potential. The region representing these conditions is called Design Space (DS) and it is represented by the yellow area of Fig. S2 of the supplementary material.

The DS for both DTX, at 0.02 and 0.08% w/v, revealed a wide area of possible final formulations. However, at 0.16% w/v DTX the area was reduced to a small fraction of space. With this information and taking into account DTX concentration values used in therapy and in other drug delivery systems [55], we proceed to analyze the response surface for a formulation at 0.08% w/v fixed DTX load. Fig. 1 shows the 2D and 3D plots of desirability with 0.08% w/v of DTX considering simultaneously the responses: size, PDI and ZP. Higher values of desirability indicate the conditions that meet the criteria described above.

It can be seen from the DS and the desirability plot that it is not possible to achieve a suitable formulation with F127 and F68 simultaneously at the 1.5% w/v level. This can be correlated with the visual findings of P3-P10, described above. These two formulations are far from the yellow area of the DS (Fig. S2) and show the lowest desirability (Fig. 1), indicating unsuitable quality attributes of the formulations. Based on these results, two formulations were chosen: one with a high proportion of F68 (named PLN1) and one with high proportion F127 (named PLN2). A resume on the final composition of this formulations is available in Table 2.

3.3. Encapsulation efficiency

The encapsulation efficiency (%EE) is a measure that determines the extent of the drug loaded into the nanocarrier. In this study, %EE was determined by the ultrafiltration-centrifugation method. The nanoparticles showed an excellent capability to encapsulate DTX with values higher than the 90% for PNL1 (95.1% SD 0.5) and PNL2 (95.6% SD 0.4). In this way, almost all of the DTX was encapsulated into the nanoparticle. Drug loading was calculated to be 1.90% for PLN1 and 1.92% for PLN2.

Table 2
Final formulations: composition PLN1 and PLN2.

Factor % (w/v)	PLN1	PLN2
DTX	0.08	0.08
CP	1	1

3.4. Physicochemical stability

The PLNs, with and without DTX, were followed during 6 months of refrigerated storage (2–5 °C), at fixed time intervals. The formulations were visually inspected and also regarding size (nm), PDI, ZP (mV) and nanoparticle concentration. Figs. 2 and S3 of the supplementary material, shows the results for the first 6 months after preparation, during which the nanoparticles proved to be stable.

During the stability tests, the formulations showed a homogenous appearance, conserving their characteristic opacity. Size fluctuations over time were not statistically significant, for any of the formulations. PDI values fluctuated between 0.18 and 0.26 over the time, without statistical significance and indicating suitable polydispersity for the formulations over 6 months storage. Nanoparticle tracking was performed to determine particle concentration. No significant changes were observed for any of the formulations, which kept the number of particles around 10^{13}/mL during the length of the study (Fig. S3). Since the nanoparticles presented elevated number of polymers in their composition, steric stabilization of the systems could be responsible for the stability of the colloidal dispersion. In this direction, the ZP fluctuations throughout the study (Fig. S3), had no significant impact on size, polydispersity or number of particles. This result confirmed the physicochemical stability of the formulations and their suitability to be applied as DDS.

3.5. Transmission Electron microscopy

After assessing the stability of the nanoparticles, we performed transmission electron microscopy of the four samples. Fig. 3 displays the micrographs of the PLN1 and PLN2 formulations, with and without DTX. The images confirmed that the nanoparticles were successfully prepared, maintaining the spherical shape with visible contours, even after DTX encapsulation, without affecting the nanoparticle integrity [51].

Using the ImageJ software, it was possible to estimate the size of the individual nanoparticles in neat PLN1 (~197 nm), DTX loaded PLN1 (~240 nm), neat PLN2 (~180 nm) and DTX-loaded PLN2 (~220 nm). These results are in the good agreement with particle diameters determined by DLS (Fig. 2). However, it is worth to mention that since TEM sample preparation requires solvent evaporation, this may cause structural distortion of the particles into clusters [56]. Since this effect causes shrinkage, distortion, overlapping or disruption of the particles, we consider TEM micrographs to give qualitative information on the nanoparticles [56]. For quantitative information, size distribution

F127	0.5	1.5
F68	1.5	0.5

nanoparticles [56]. For quantitative information size distribution, analysis through analytical techniques (such as DLS and NTA) are more reliable.

59

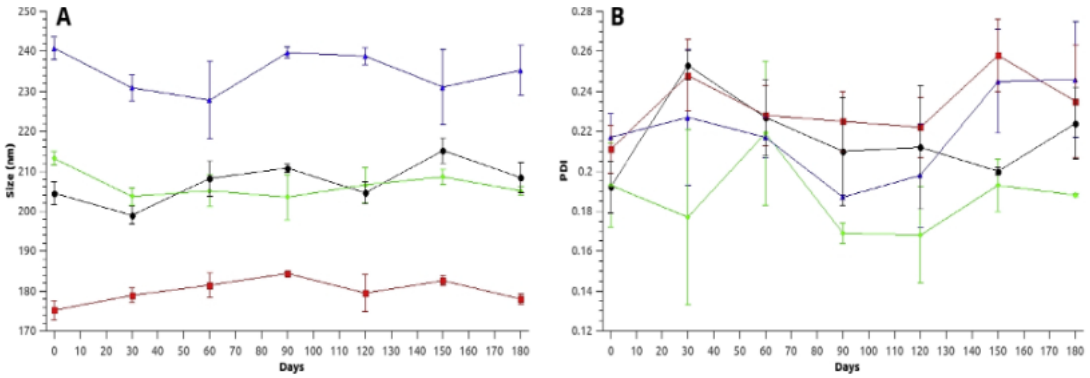

Fig. 2. Physicochemical stability in terms of Size (A) and PDI (B) for neat PLN1 (blue) and PLN2 (green) and drug-loaded PLN1 (red) and PLN2 (black). Measurements were performed every month up to six months (180 days).

3.6. Release kinetics analysis

The modulation of drug release kinetics is often a goal when developing a DDS [57]. Taking into account the EPR effect (enabling the accumulation of the nanoparticles into the tumor tissue), the sustained release of the drug encapsulated in nanoparticles, such as the developed in this work, could improve the therapeutic effect of the drug, administered at lower doses [57]. In order to evaluate the capability of the formulations to modulate drug delivery, *in vitro* release experiments were performed as described in the methods section. Fig. 4 shows the release profile for DTX in solution and encapsulated in PLN1 and PLN2 formulations, over 24 hs. For the free drug, a slow release of DTX is observed in the first 15 h of the study, and total release was achieved after 24 h. Using the KinetDS software, this release kinetics was established as a Weibull distribution (solid green line in Fig. 10) and was attributed to the extremely low solubility of the drug. For the

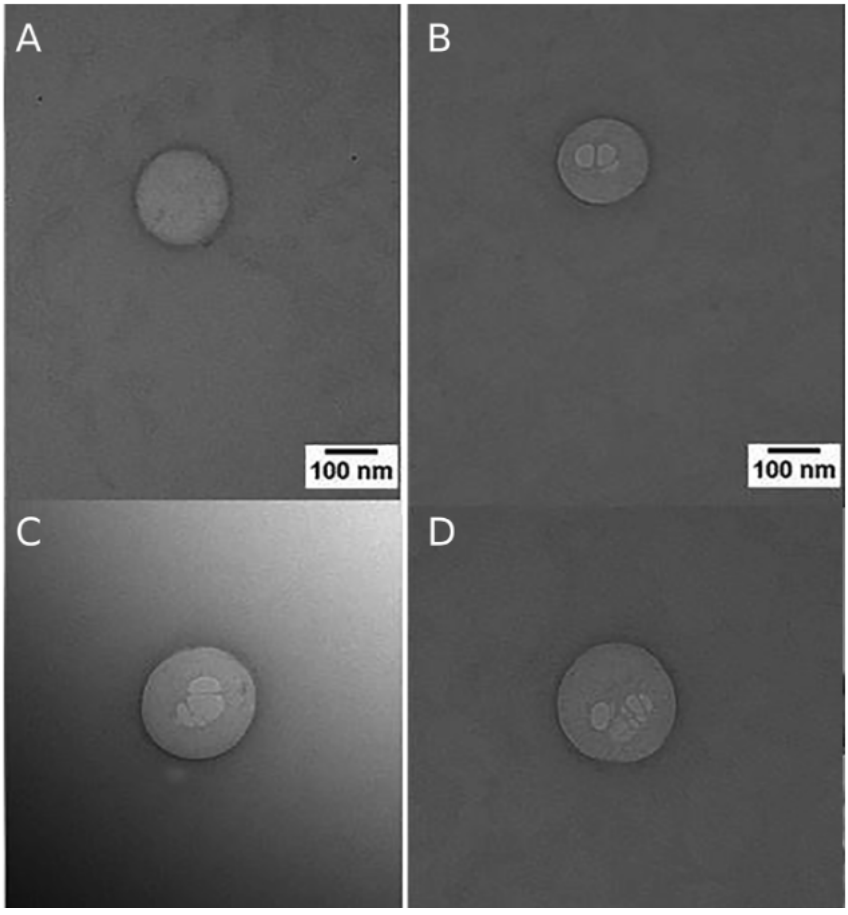

Fig. 3. TEM images of neat PLN1 (A), PLN2 (B) and DTX-loaded PLN1 (C), PLN2 (D) in 100,000 x magnification.

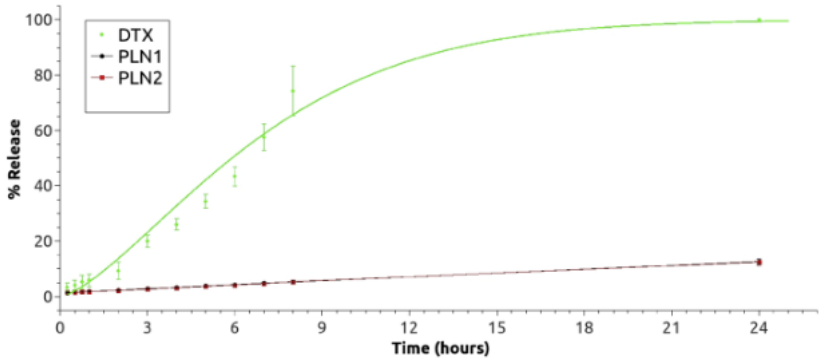

Fig. 4. Profiles of *in vitro* DTX cumulative release, as determined by dialysis equilibrium at 37 °C. In green: free DTX (0.8 mg/mL); in black and red, optimized (PLN1 and PLN2, respectively) DTX loaded-nanoparticles.

formulations, a slow release was observed during the length of the study, yielding approximately 13% of released drug after 24 hs. This release corresponded to a linear distribution and so, to a first order release kinetics during the time of the study. These results are in good agreement with release studies with DTX in other nanoparticulated systems [55] suggesting that the PLNs are suitable for the sustained release of DTX for many days. Further insights on this behavior will be addressed in Section 3.8.

It is important to remark that under in-vivo physiological conditions the release kinetics can be modified by numerous factors. In particular, the tumoral microenvironment has unique features, such as slow blood flow, higher local temperature and lower pH, that can modulate it [58]. Taking advantage of the EPR effect, these newly developed nanoparticles could accumulate into the tumoral mass, where the temperature and pH changes would accelerate its degradation and boost DTX local release. Furthermore, once at the site, highly active tumoral cancer cells could internalize these nanoparticles, releasing the drug within to the cell [59].

3.7. Structural characterization

Despite the recognized difficulty to elucidate the physical state of the encapsulated molecules in lipid systems, we employed a set of structural characterization methods (DSC, XRD, ATR-FTIR and MD) for the individual components and PLN with and without DTX, attempting to understand the structural organization of the novel system under a qualitative perspective. Given that both PLNs share the same components, in the following sections we show the results obtained with one of the formulations (PNL2) with and without DTX, as an example.

3.7.1. DSC analysis

Fig. 5A exhibits the calorimetric profile of the excipients and neat PLN, which were very similar, corresponding to the endothermic peaks of their melting points, placed from 54 to 58 °C [51,60]. These results support the approach used at the initial steps of the PLN elaboration, as explained in the 3.1 section. In Fig. 4B, the DTX thermogram showed an endothermic peak detected around 165 °C, corresponding to the melting point of the drug [61,62]. This peak is not present in the nanoparticle drug-loaded spectrum. The thermograms of the PLN2 formulation, with and without DTX showed very similar profiles, with a single endothermic peak due to the melting point of the structural excipients that did not change upon drug encapsulation.

arrangement of the drug [63]. For comparison purposes, the DRX spectrum of each of the pure excipients is presented in Fig. S4 of the supplementary material. The neat PLN2 and DTX loaded formulations exhibited similar diffractogram profiles suggesting that DTX entrapment did not disturb the molecular organization of the nanoparticle. Furthermore, no crystalline peaks of DTX were observed in the PLN2/DTX peaks profile, followed by its less crystallinity than neat PLN2 drug-free diffractogram formulations, suggesting that interactions took place among the excipients.

3.7.3. ATR-FTIR analysis

The infrared spectroscopy technique was used to get qualitative insights on the drug loaded nanoparticles. The FTIR frequencies and their assignments are shown in Table S6 of the supplementary material. Fig. 7A shows the FTIR spectra of PLN components: PL F127 (orange), F68 (green) and CP (blue). The spectra of F127 and F68 are quite similar between them, with the main bands at 1466 and 1468 cm^{-1} (νCH2), 1340 and 1344 cm-1 (νO-C-O), 1280 and 1278 cm^{-1} (νO-C-O), 963 and 965 cm^{-1} (δCH), 840 and 842 cm^{-1} (δCH) [53,54]. For CP, the main spectrum bands are at 2915 (νCH), 2850 (νO-CH2), and 1730 (νC = O) cm^{-1} [55]. The ATR-FTIR spectrum of the PLN (black) presented slight shifts in comparison to that of its individual components, e.g. ν_{CH} band from 2915 (CP) to 2919 cm^{-1}, suggesting changes in the local environment of cetyl palmitate inside the nanoparticle. In previously reported CP-based SLNs, the ν_{CH} band was found at 2916 cm^{-1} reinforcing the novelty of the PLN discussed developed in this work [64].

Once the neat PLN FTIR spectrum was characterized, the effects of the DTX in this new polymer-lipid milieu was assessed. In Fig. 7B FTIR spectra of DTX, and PLN2 (with and without DTX) is disclosed. In its free form, DTX spectrum show a broad band centered in 3369 cm^{-1} assigned to ν_{N-H} and ν_{OH}; a wide band at 1710 cm^{-1} assigned to $\nu_{C=O}$, and a band at 1596 cm^{-1}, attributed to the amine free group vibration (δ_{N-H}) [65]. Since DTX is present at small percentages in the PLN2 formulation, it could be difficult to assess shifts in the frequencies of the bands assigned to the drug, with this technique. However, DTX changes on the PLN2 structure could be significant, as explored in the factorial analysis section of this work. In our study, the overall FTIR spectrum of PLN2/DTX is very similar to that of the neat PLN2 formulation, showing that no significant changes in the nanocarrier environment occurs upon drug encapsulation.

3.7.2. DRX analysis

DRX and DSC are complementary techniques that can be applied to explore the polymorphic structures of nanocarrier systems upon drug encapsulation. The diffractogram of pure DTX (Fig. 6) detected typical sharp peaks in 8°, 11°, 14°, and 17°, confirming its crystalline

3.8. Molecular dynamics simulations

Encapsulation, release kinetics and structural analysis of the formulations yielded strong evidence that DTX is inside the polymer-lipid matrix of the PLN. However, with experimental techniques, it is difficult to access details (at the molecular level) of the DTX insertion within

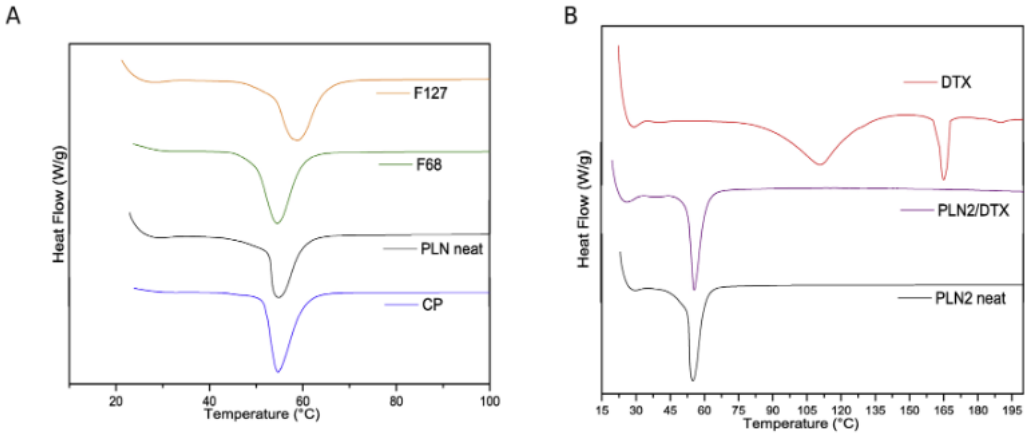

Fig. 5. DSC analyses of A) excipients and PLN2 drug-free formulation and B) DTX, PLN2/DTX, and PLN2 drug-free formulations.

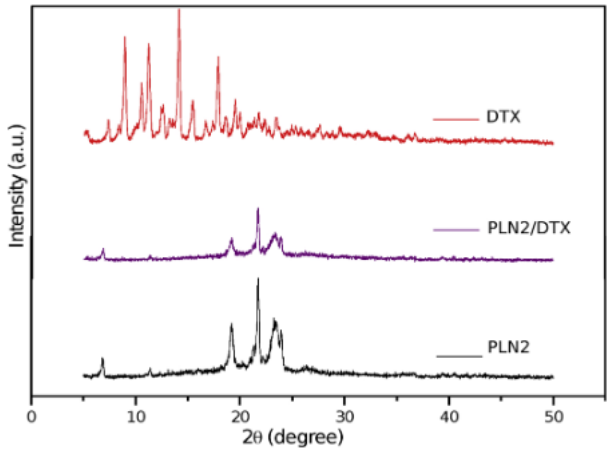

Fig. 6. XRD patterns of DTX, PLN2/DTX, and PLN2 drug-free formulations.

the nanoparticle. In this direction, computational simulations - in particular Molecular Dynamics simulations – could shed light to the molecular interplay of the drug in the nanoparticle core matrix [66].

As a first step, we aim to understanding the internal structure of the newly developed PLNs. In this direction, considering that the main components of the inner core are the cetyl-palmitate and the drug, we considered a cubic simulation box of ~ $(17\,nm)^3$, containing 50 molecules of paclitaxel and 5000 molecules of CP as schematized in Fig. S5 of the Supplementary Material. Because we focused our study in the innermost core of the nanoparticles, were a mayor proportion of CP is supposed to be present, the explicit poloxamer contribution in this region was neglected, and therefore not included in the simulations. It could be interesting to remark that PPO blocks of the PL, that could be present at hydrophobic core, are represented by similar hydrophobic CG beads as the ones proposed here for the MFF CP bead [26,45,67]. PTX force-field parameters were previously reported and validated [47]. In this way, for the simulation studies, Paclitaxel (PTX) instead DTX, was chosen as a model drug due to its major structural and physicochemical similarities between them [68,69]. For the CG CP, we based our model in the MFF parametrization of lipids, and given its floppy nature, no special restrains were applied to its structure (see Supplementary Material). The drug: excipient proportion was estimated from NTA measurements (results not shown).

Simulations were started from three different initial configurations, randomizing the distribution of PTX throughout the simulation box and run up to 2μs. In Fig. 8A, B and C representative snapshots for each case at 2 μs are shown. Each PTX molecule is represented in different color and the CP are removed for visualization purpose. As it can be observed, PTX molecules appeared to be forming clusters inside the nanoparticle core. Given that PTX and DTX have similar physicochemical and structural properties [68,69], such distribution in the core of the PLN is supported by the structural experiments performed in this work

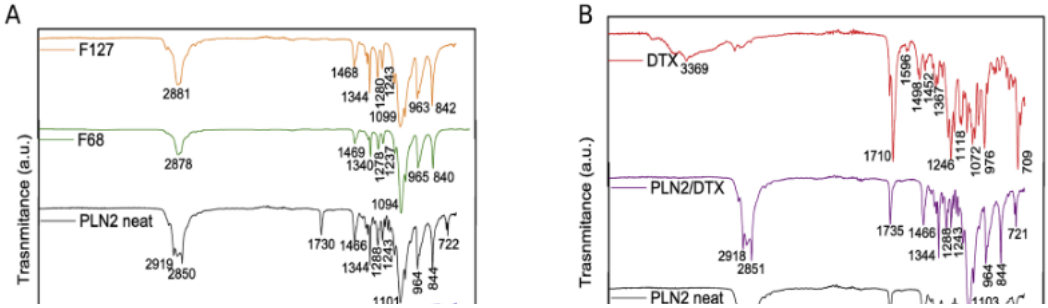

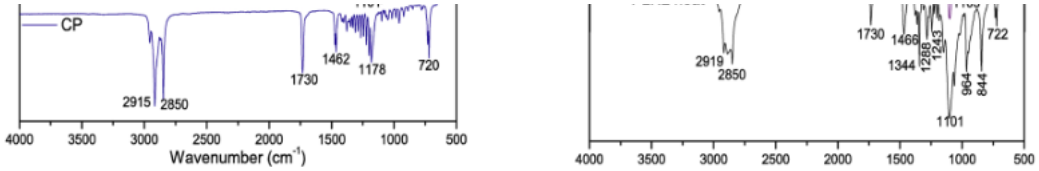

Fig. 7. A- FTIR-ATR spectra of the excipients and the PLN2 formulation. B- FTIR-ATR spectra of DTX, PLN2, and PLN2/DTX formulations.

62

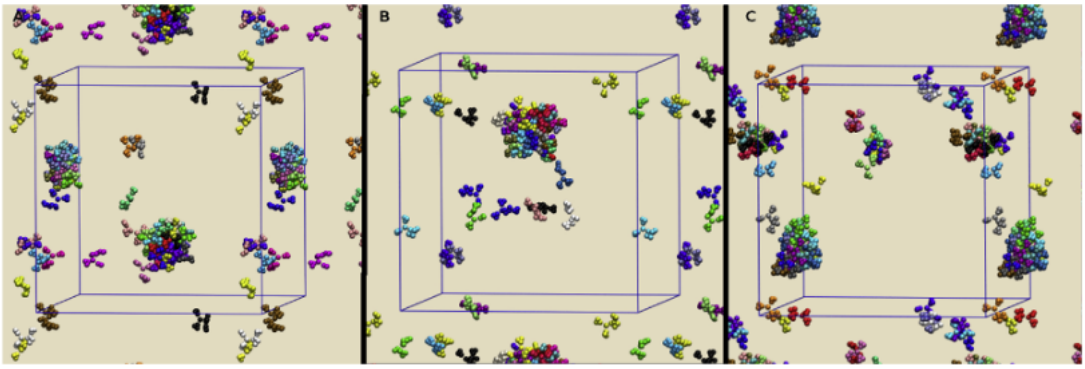

Fig. 8. Snapshots of 3 PTX-CP simulated systems (A, B and C) at the end of the 2 μs simulations. The simulation box is shown in blue, and periodic boundary condition representations at the x,y and z axes were used to show paclitaxel (individually colored). CP molecules and are not shown for visualization purposes. Paclitaxel was used as a model of docetaxel.

and also gives an insight on the observed encapsulation and release kinetics for both PLN formulations.

From the results of section 3.6, we observed that a slower and sustained release was present for the DTX encapsulated in the nanoparticles. In this direction, insights from MD simulations suggest that this clustering inside the nanoparticle core would be responsible for this release kinetics.

4. Conclusions

A DTX polymer-lipid nanostructured carrier (PLN) was rationally developed and optimized with the use of factorial design. We firstly explored the possibility of formulating a nanoparticle using low amounts of each component. The novelty here was to obtain a formulation with lower amount of total excipients in comparison with available formulations of solid lipid nanoparticles. Besides, with the chosen proportion of poloxamers used, an active role for that polymer was intended within the formulation. With the factorial design approach, two formulations were selected, that contained different proportions of F127 and F68. In both cases, the optimized PLNs were able to encapsulate a high amount of DTX. Different techniques were used to characterize the physicochemical properties of these nanocarriers. Altogether, these techniques agreed that the PLNs kept their structural features upon insertion of DTX into the polymeric-lipid matrix. PLNs provided sustained *in vitro* release of DTX for more than 24 h. Through molecular dynamics simulations we were able to capture some key features of the behavior of the drug in the innermost core such as their aggregation that could explain the observed release kinetics.

In addition to the functionalization of the PLNs provided by the polymers, the size of the nanoparticles made the formulation suitable to take advantage of the EPR effect, improving tumor targeting of DTX. In this way, the attributes of this novel PLN/DTX system points out it as a promising formulation to be tested for the cancer treatment. To advance in this direction, further *in vitro* and *in vivo* studies are fundamental, and they will be assessed in a future work. These techniques could help identifying the more efficient of the two optimized formulations. Also, further computer simulations studies could shed light into the complex structure of this kind of nanoparticle, difficult to access with experi-

Brazilian funding agency (#14/25372-0 and #14/14457-5). MP have been partially supported by grants ANPCyT PICT 2014- 3653 and PIP CONICET 0131-2014. JMRA have been partially supported by a grant from Florencio Fiorini Foundation.

Appendix A. Supplementary data

Supplementary material related to this article can be found, in the online version, at doi:https://doi.org/10.1016/j.colsurfb.2018.11.077.

References

[1] K.D. Miller, R.L. Siegel, C.C. Lin, et al., Cancer treatment and survivorship statistics, 2016, CA Cancer J. Clin. 66 (2016) 271–289, https://doi.org/10.3322/caac.21349.
[2] E. Saloustros, V. Georgoulias, Docetaxel in the treatment of advanced non-small-cell lung cancer, Expert Rev. Anticancer Ther. 8 (2008) 1207–1222, https://doi.org/10.1586/14737140.8.8.1207.
[3] E. Saloustros, D. Mavroudis, V. Georgoulias, Paclitaxel and docetaxel in the treatment of breast cancer, Expert Opin. Pharmacother. 9 (2008) 2603–2616, https://doi.org/10.1517/14656566.9.15.2603.
[4] A. Montero, F. Fossella, G. Hortobagyi, V. Valero, Docetaxel for treatment of solid tumours: a systematic review of clinical data, Lancet Oncol. 6 (2005) 229–239, https://doi.org/10.1016/S1470-2045(05)70094-2.
[5] G.J. Berchem, M. Bosseler, N. Mine, B. Avalosse, Nanomolar range docetaxel treatment sensitizes MCF-7 cells to chemotherapy induced apoptosis, induces G2M arrest and phosphorylates bcl-2, Anticancer Res. 19 (1999) 535–540.
[6] H. Hernández-Vargas, J. Palacios, G. Moreno-Bueno, Molecular profiling of docetaxel cytotoxicity in breast cancer cells: uncoupling of aberrant mitosis and apoptosis, Oncogene 26 (2007) 2902–2913, https://doi.org/10.1038/sj.onc.1210102.
[7] W. Huang, J. Zhang, H.C. Dorn, C. Zhang, Assembly of bio-nanoparticles for double controlled drug release, PLoS One 8 (2013), https://doi.org/10.1371/journal.pone.0074679.
[8] I. Kuppens, Current state of the art of new tubulin inhibitors in the clinic, Curr. Clin. Pharmacol. 1 (2006) 57–70, https://doi.org/10.2174/157488406775268200.
[9] F.K. Engels, R.A.A. Mathot, J. Verweij, Alternative drug formulations of docetaxel: a review, Anticancer Drugs 18 (2007) 95–103, https://doi.org/10.1097/CAD.0b013e3280113338.
[10] N. Katsumata, Docetaxel: an alternative taxane in ovarian cancer, Br. J. Cancer 89 (2003) S9–S15, https://doi.org/10.1038/sj.bjc.6601495.
[11] J. Baker, J. Ajani, F. Scotté, et al., Docetaxel-related side effects and their management, Eur. J. Oncol. Nurs. 13 (2009) 49–59, https://doi.org/10.1016/j.ejon.2008.10.003.
[12] R. Agrawal, A. Shanavas, S. Yadav, et al., Polyelectrolyte coated polymeric nanoparticles for controlled release of docetaxel, J. Biomed. Nanotechnol. 8 (2012) 19–28, https://doi.org/10.1166/jbn.2012.1355.

structure of this kind of nanoparticle, difficult to access with experimental techniques.

Conflict of interest

The authors declare no conflicts of interest.

Acknowledgements

EP have been partially supported by grants from the FAPESP

[13] S. Saremi, R. Dinarvand, A. Kebriaeezadeh, et al., Enhanced oral delivery of docetaxel using thiolated chitosan nanoparticles: preparation, in vitro and in vivo studies, Biomed Res. Int. 2013 (2013), https://doi.org/10.1155/2013/150478.
[14] P. Rafiei, A. Haddadi, Docetaxel-loaded PLGA and PLGA-PEG nanoparticles for intravenous application: pharmacokinetics and biodistribution profile, Int. J. Nanomed. 12 (2017) 935–947, https://doi.org/10.2147/IJN.S121881.
[15] C. Schwarz, W. Mehnert, J.S. Lucks, R.H. Müller, Solid lipid nanoparticles (SLN) for controlled drug delivery. I. Production, characterization and sterilization, J. Control. Release 30 (1994) 83–96, https://doi.org/10.1016/0168-3659(94)90047-7.
[16] E.C. Umeyor, F.C. Kenechukwu, J.D. Ogbonna, et al., Preparation of novel solid lipid microparticles loaded with gentamicin and its evaluation in vitro and in vivo,

J. Microencapsul. 29 (2012) 296–307, https://doi.org/10.3109/02652048.2011.651495.
[17] Q. Yuan, J. Han, W. Cong, et al., Docetaxel-loaded solid lipid nanoparticles suppress breast cancer cells growth with reduced myelosuppression toxicity, Int. J. Nanomed. 9 (2014) 4829–4846, https://doi.org/10.2147/IJN.S70919.
[18] D. Zheng, D. Li, X. Lu, Z. Feng, Enhanced antitumor efficiency of docetaxel-loaded nanoparticles in a human ovarian xenograft model with lower systemic toxicities by intratumoral delivery, Oncol. Rep. 23 (2010) 717–724, https://doi.org/10.3892/or-00000689.
[19] M.L. Cacicedo, G.A. Islan, I.E. León, et al., Bacterial cellulose hydrogel loaded with lipid nanoparticles for localized cancer treatment, Colloids Surf. B Biointerfaces 170 (2018) 596–608, https://doi.org/10.1016/j.colsurfb.2018.06.056.
[20] S. Azzi, J.K. Hebda, J. Gavard, Vascular permeability and drug delivery in cancers, Front. Oncol. 3 (2013) 211, https://doi.org/10.3389/fonc.2013.00211.
[21] S.D. Steichen, M. Caldorera-Moore, N.A. Peppas, A review of current nanoparticle and targeting moieties for the delivery of cancer therapeutics, Eur. J. Pharm. Sci. 48 (2013) 416–427.
[22] H. Maeda, H. Nakamura, J. Fang, The EPR effect for macromolecular drug delivery to solid tumors: improvement of tumor uptake, lowering of systemic toxicity, and distinct tumor imaging in vivo, Adv. Drug Deliv. Rev. 65 (2013) 71–79.
[23] H. Kobayashi, R. Watanabe, P.L. Choyke, Improving conventional enhanced permeability and retention (EPR) effects; what is the appropriate target? Theranostics 4 (2014) 81–89.
[24] H. Weyhers, S. Ehlers, H. Hahn, et al., Solid lipid nanoparticles (SLN)–effects of lipid composition on in vitro degradation and in vivo toxicity, Pharmazie 61 (2006) 539–544.
[25] A. Pitto-Barry, N.P.E. Barry, Pluronic® block-copolymers in medicine: from chemical and biological versatility to rationalisation and clinical advances, Polym. Chem. 5 (2014) 3291–3297, https://doi.org/10.1039/C4PY00039K.
[26] I. Wood, M.F. Martini, J.M.R. Albano, et al., Coarse grained study of pluronic F127: comparison with shorter co-polymers in its interaction with lipid bilayers and self-aggregation in water, J. Mol. Struct. 1109 (2016) 106–113, https://doi.org/10.1016/j.molstruc.2015.12.073.
[27] A.V. Kabanov, E.V. Batrakova, V.Y. Alakhov, Pluronic® block copolymers for overcoming drug resistance in cancer, Adv. Drug Deliv. Rev. 54 (2002) 759–779, https://doi.org/10.1016/S0169-409X(02)00047-9.
[28] A.K. Sharma, L. Zhang, S. Li, et al., Prevention of MDR development in leukemia cells by micelle-forming polymeric surfactant, J. Control. Release 131 (2008) 220–227, https://doi.org/10.1016/j.jconrel.2008.07.031.
[29] A. Venne, S. Li, R. Mandeville, et al., Hypersensitizing effect of pluronic L61 on cytotoxic activity, transport, and subcellular distribution of doxorubicin in multiple drug- resistant cells, Cancer Res. 56 (1996) 3626–3629.
[30] H. Lage, ABC-transporters: implications on drug resistance from microorganisms to human cancers, Int. J. Antimicrob. Agents 22 (2003) 188–199.
[31] Z. Chen, T. Shi, L. Zhang, et al., Mammalian drug efflux transporters of the ATP binding cassette (ABC) family in multidrug resistance: a review of the past decade, Cancer Lett. 370 (2016) 153–164.
[32] E.V. Batrakova, S. Li, S.V. Vinogradov, et al., Mechanism of pluronic effect on P-glycoprotein efflux system in blood-brain barrier: contributions of energy depletion and membrane fluidization, J. Pharmacol. Exp. Ther. 299 (2001) 483–493.
[33] C.K. Song, P. Balakrishnan, C.-K. Shim, et al., Enhanced in vitro cellular uptake of P-gp substrate by poloxamer-modified liposomes (PMLs) in MDR cancer cells, J. Microencapsul. 28 (2011) 575–581, https://doi.org/10.3109/02652048.2011.599436.
[34] Z. Wei, S. Yuan, J. Hao, X. Fang, Mechanism of inhibition of P-glycoprotein mediated efflux by Pluronic P123/F127 block copolymers: relationship between copolymer concentration and inhibitory activity, Eur. J. Pharm. Biopharm. 83 (2013) 266–274, https://doi.org/10.1016/j.ejpb.2012.09.014.
[35] D.Y. Alakhova, A.V. Kabanov, Pluronics and MDR reversal: an update, Mol. Pharm. 11 (2014) 2566–2578, https://doi.org/10.1021/mp500298q.
[36] D. Jain, R. Athawale, A. Bajaj, et al., Studies on stabilization mechanism and stealth effect of poloxamer 188 onto PLGA nanoparticles, Colloids Surf. B Biointerfaces 109 (2013) 59–67, https://doi.org/10.1016/j.colsurfb.2013.03.027.
[37] L. Mayol, C. Serri, C. Menale, et al., Curcumin loaded PLGA–poloxamer blend nanoparticles induce cell cycle arrest in mesothelioma cells, Eur. J. Pharm. Biopharm. 93 (2015) 37–45, https://doi.org/10.1016/j.ejpb.2015.03.005.
[38] S.-D. Li, L. Huang, Stealth nanoparticles: high density but sheddable PEG is a key for tumor targeting, J. Control. Release 145 (2010) 178–181, https://doi.org/10.1016/j.jconrel.2010.03.016.
[39] R. Gref, M. Lück, P. Quellec, et al., 'Stealth' corona-core nanoparticles surface modified by polyethylene glycol (PEG): influences of the corona (PEG chain length
[43] P. Nahak, G. Karmakar, B. Roy, et al., Physicochemical studies on local anaesthetic loaded second generation nanolipid carriers, RSC Adv. 5 (2015) 26061–26070, https://doi.org/10.1039/C4RA16434B.
[44] H. Chen, Y. Wang, Y. Zhai, et al., Development of a ropivacaine-loaded nanostructured lipid carrier formulation for transdermal delivery, Colloids Surf. A Physicochem. Eng. Asp. 465 (2015) 130–136, https://doi.org/10.1016/j.colsurfa.2014.10.046.
[45] S.J. Marrink, H.J. Risselada, S. Yefimov, et al., The MARTINI force field: coarse grained model for biomolecular simulations, J. Phys. Chem. B 111 (2007) 7812–7824, https://doi.org/10.1021/jp071097f.
[46] S.O. Yesylevskyy, L.V. Schäfer, D. Sengupta, S.J. Marrink, Polarizable water model for the coarse-grained MARTINI force field, PLoS Comput. Biol. 6 (2010) 1–17, https://doi.org/10.1371/journal.pcbi.1000810.
[47] R. Namgung, Y. Mi Lee, J. Kim, et al., Poly-cyclodextrin and poly-paclitaxel nanoassembly for anticancer therapy, Nat. Commun. 5 (2014), https://doi.org/10.1038/ncomms4702.
[48] H.J.C. Berendsen, J.P.M. Postma, W.F. van Gunsteren, et al., Molecular dynamics with coupling to an external bath, J. Chem. Phys. 81 (1984) 3684–3690, https://doi.org/10.1063/1.448118.
[49] H.J.C. Berendsen, D. van der Spoel, R. van Drunen, GROMACS: a message passing parallel molecular dynamics implementation, Comp. Phys. Comm. 91 (1995) 43–56, https://doi.org/10.1016/0010-4655(95)00042-E.
[50] R.H. Müller, K. Mäder, S. Gohla, Solid lipid nanoparticles (SLN) for controlled drug delivery - a review of the state of the art, Eur. J. Pharm. Biopharm. 50 (2000) 161–177.
[51] L.N.M. Ribeiro, M. Franz-Montan, M.C. Breitkreitz, et al., Nanostructured lipid carriers as robust systems for topical lidocaine-prilocaine release in dentistry, Eur. J. Pharm. Sci. 93 (2016) 192–202, https://doi.org/10.1016/j.ejps.2016.08.030.
[52] L.N.M. Ribeiro, M.C. Breitkreitz, V.A. Guilherme, et al., Natural lipids-based NLC containing lidocaine: from pre-formulation to in vivo studies, Eur. J. Pharm. Sci. 106 (2017) 102–112, https://doi.org/10.1016/j.ejps.2017.05.060.
[53] B. Rodenak-Kladniew, G.A. Islan, M.G. de Bravo, et al., Design, characterization and in vitro evaluation of linalool-loaded solid lipid nanoparticles as potent tool in cancer therapy, Colloids Surf. B Biointerfaces 154 (2017) 123–132, https://doi.org/10.1016/j.colsurfb.2017.03.021.
[54] F. Yan, C. Zhang, Y. Zheng, et al., The effect of poloxamer 188 on nanoparticle morphology, size, cancer cell uptake, and cytotoxicity, Nanomed. Nanotechnol. Biol. Med. 6 (2010) 170–178, https://doi.org/10.1016/j.nano.2009.05.004.
[55] M. Jin, S. Piao, T. Jin, et al., Improved anti-tumor efficiency against prostate cancer by docetaxel-loaded PEG-PCL micelles, J. Huazhong Univ. Sci. Technol. Med. Sci. 34 (2014) 66–75, https://doi.org/10.1007/s11596-014-1233-0.
[56] O.A. Jensen, J.U. Prause, H. Laursen, Shrinkage in preparatory steps for SEM. A study on rabbit corneal endothelium, Albrecht Von Graefes Arch. Klin. Exp. Ophthalmol. 215 (1981) 233–242.
[57] L. Feng, R.J. Mumper, A critical review of lipid-based nanoparticles for taxane delivery, Cancer Lett. 334 (2013) 157–175, https://doi.org/10.1016/j.canlet.2012.07.006.
[58] F.R. Balkwill, M. Capasso, T. Hagemann, The tumor microenvironment at a glance, J. Cell. Sci. 125 (2012) 5591–5596, https://doi.org/10.1242/jcs.116392.
[59] S. Martins, S. Costa-Lima, T. Carneiro, et al., Solid lipid nanoparticles as intracellular drug transporters: an investigation of the uptake mechanism and pathway, Int. J. Pharm. 430 (2012) 216–227, https://doi.org/10.1016/j.ijpharm.2012.03.032.
[60] N. Kolašinac, K. Kachrimanis, I. Homšek, et al., Solubility enhancement of desloratadine by solid dispersion in poloxamers, Int. J. Pharm. 436 (2012) 161–170, https://doi.org/10.1016/j.ijpharm.2012.06.060.
[61] H. Singh, R. Sharma, M. Joshi, et al., Transmucosal delivery of Docetaxel by mucoadhesive polymeric nanofibers, Artif. Cells Nanomed. Biotechnol. 43 (2015) 263–269, https://doi.org/10.3109/21691401.2014.885442.
[62] X. Zeng, W. Tao, L. Mei, et al., Cholic acid-functionalized nanoparticles of star-shaped PLGA-vitamin E TPGS copolymer for docetaxel delivery to cervical cancer, Biomaterials 34 (2013) 6058–6067, https://doi.org/10.1016/j.biomaterials.2013.04.052.
[63] L. Zaske, M.-A. Perrin, C. Daiguebonne, O. Guillou, Docetaxel (Taxotere® trihydrate) forms: crystal structure determination from XRPD & XRSCD data, Mater. Sci. Forum. (2004) 443–444 411–0. doi: 10.4028/ www.scientific.net/MSF.443-444.411.
[64] A. Saupe, K.C. Gordon, T. Rades, Structural investigations on nanoemulsions, solid lipid nanoparticles and nanostructured lipid carriers by cryo-field emission scanning electron microscopy and Raman spectroscopy, Int. J. Pharm. 314 (2006) 56–62, https://doi.org/10.1016/j.ijpharm.2006.01.022.

and surface density) and of the core composition on phagocytic uptake and plasma protein adsorption, Colloids Surf. B Biointerfaces 18 (2000) 301–313, https://doi.org/10.1016/S0927-7765(99)00156-3.

[40] A. Loureiro, J. Noro, A.S. Abreu, et al., Absence of albumin improves in vitro cellular uptake and disruption of poloxamer 407-Based nanoparticles inside Cancer cells, Mol. Pharm. 15 (2018) 527–535, https://doi.org/10.1021/acs.molpharmaceut.7b00893.

[41] C.M. Moraes, E. Paula, de, A.H. Rosa, L.F. Fraceto, Validação de metodologia analítica por cromatografia líquida de alta eficiência para quantificação de bupivacaína (S75-R25) em nanoesferas de poli(lactí deo-co-glicolí deo), Quim. Nova 31 (2008) 2152–2155, https://doi.org/10.1590/S0100-40422008000800040.

[42] G.H. Rodrigues da Silva, L.N.M. Ribeiro, H. Mitsutake, et al., Optimised NLC: a nanotechnological approach to improve the anaesthetic effect of bupivacaine, Int. J. Pharm. 529 (2017) 253–263, https://doi.org/10.1016/j.ijpharm.2017.06.066.

[65] X. Fan, J. Chen, Q. Shen, Docetaxel–nicotinamide complex-loaded nanostructured lipid carriers for transdermal delivery, Int. J. Pharm. 458 (2013) 296–304, https://doi.org/10.1016/j.ijpharm.2013.10.036.

[66] J.M.R. Albano, Paula E. de, M. Pickholz, molecular dynamics simulations to study drug delivery systems, Mol. Dyn. InTech. (2018), https://doi.org/10.5772/intechopen.75748.

[67] I. Wood, J.M.R. Albano, P.L.O. Filho, et al., A sumatriptan coarse-grained model to explore different environments: interplay with experimental techniques, Eur. Biophys. J. (2018), https://doi.org/10.1007/s00249-018-1278-2.

[68] R. Pazdur, A.P. Kudelka, J.J. Kavanagh, et al., The taxoids: paclitaxel (Taxol) and docetaxel (Taxotere), Cancer Treat. Rev. 19 (1993) 351–386.

[69] J.-S. Baek, C.-W. Cho, Comparison of solid lipid nanoparticles for encapsulating paclitaxel or docetaxel, J. Pharm. Investig. 45 (2015) 625–631, https://doi.org/10.1007/s40005-015-0182-3.